Particle & Particle Systems Characterization
www.particle-journal.com

Combination of HAADF-STEM and ADF-STEM Tomography for Core–Shell Hybrid Materials

*Kadir Sentosun, Marta N. Sanz Ortiz, K. Joost Batenburg, Luis M. Liz-Marzán, and Sara Bals**

Characterization of core–shell type nanoparticles in 3D by transmission electron microscopy (TEM) can be very challenging. Especially when both heavy and light elements coexist within the same nanostructure, artifacts in the 3D reconstruction are often present. A representative example would be a particle comprising an anisotropic metallic (Au) nanoparticle coated with a (mesoporous) silica shell. To obtain a reliable 3D characterization of such an object, a dose-efficient strategy is proposed to simultaneously acquire high-angle annular dark-field scanning TEM and annular dark-field tilt series for tomography. The 3D reconstruction is further improved by applying an advanced masking and interpolation approach to the acquired data. This new methodology enables us to obtain high-quality reconstructions from which also quantitative information can be extracted. This approach is broadly applicable to investigate hybrid core–shell materials.

1. Introduction

Over the last decades, electron tomography has evolved into a standard technique to investigate the 3D structure of a broad range of (nano)materials.[1–6] To reconstruct the 3D structure of an object from its 2D projections, a monotonic relationship between image intensity and mass thickness is required.[1] When applying electron tomography to crystalline solids, diffraction contrast must therefore be avoided.[7] Indeed, diffraction contrast depends on the orientation of the object with respect to the electron beam and therefore the projection requirement for electron tomography is not fulfilled.[1] As a consequence, artifacts will occur in the final 3D reconstruction.[8,9] This is one of the main reasons why electron tomography in materials science is mostly based on high angle annular dark field scanning transmission electron microscopy (HAADF-STEM).[1,10] For each composition, the intensity of the HAADF-STEM images changes monotonically with specimen thickness thus fulfilling the projection requirement. To obtain 3D reconstructions from HAADF-STEM tilt series, reconstruction algorithms such as the simultaneously iterative reconstruction technique (SIRT),[11] total variation minimization,[12,13] and the discrete algebraic reconstruction technique[14] are currently used. Also for samples that consist of more than one type of element, HAADF-STEM tomography is very valuable since not only morphological but also chemical information can be extracted.[10] However, for samples in which elements with a high and low atomic number (Z) are simultaneously present, data acquisition becomes even more challenging. Since the intensity is strongly dependent on the atomic number,[10] a high difference in Z in the material leads to a large difference in the collected signal that is not always possible to cover with detector's dynamic range. Therefore, some areas of the image can be either over- or undersaturated. This situation is often encountered when investigating core–shell hybrid materials such as nanoparticles encapsulated by a lighter matrix. In this paper, we propose an improved approach to obtain reliable 3D reconstructions for these systems, which requires optimization of both the acquisition technique and the reconstruction algorithm. During the acquisition, HAADF-STEM images are acquired using different collection angles through the simultaneous use of different (HA)ADF detectors. Prior to the reconstruction, advanced masking and interpolation will be applied. As an example, we focus here on the reconstruction of a pentatwinned (PTW) Au nanorod coated with a mesoporous silica shell. These types of materials are of great interest due to applications in catalysis, biosensing and nonlinear optics.[15–18] Our results are

K. Sentosun, Prof. S. Bals
EMAT-University of Antwerp
Groenenborgerlaan 171, B-2020 Antwerp, Belgium
E-mail: Sara.bals@uantwerpen.be
Dr. M. N. Sanz Ortiz, Prof. L. M. Liz-Marzán
Bionanoplasmonics Laboratory
CIC biomaGUNE
Paseo de Miramón 182, 20009 Donostia-San Sebastián, Spain
Prof. K. J. Batenburg
Centrum Wiskunde and Informatica
Scientific Computing Group (MAC2.1)
Science Park 123, NL-1098XG Amsterdam, The Netherlands
Prof. K. J. Batenburg
Vision Lab
Department of Physics
University of Antwerp
Universiteitsplein 1 (CDE, N1.11), B-2610 Wilrijk, Belgium
Prof. K. J. Batenburg
Mathematical Institute
Leiden University
Niels Bohrweg 1, 2300 RA Leiden, The Netherlands
Prof. L. M. Liz-Marzán
Ikerbasque
Basque Foundation for Science
48013 Bilbao, Spain

DOI: 10.1002/ppsc.201500097

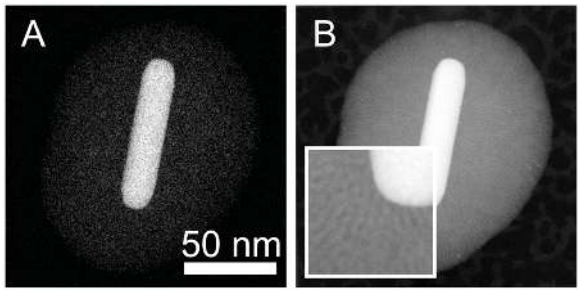

Figure 1. TEM image of a PTW Au@SiO_2 particle. A) The image was acquired using HAADF-STEM. The core can be clearly seen but the intensity from the shell is too low. B) The image was acquired using ADF STEM, showing that the intensity from the SiO_2 shell becomes prominent.

equally applicable to other hybrid nanosystems such as coated biotemplates, porous materials loaded with nanoparticles or carbon nanotubes that are covered with an inorganic layer.

2. Results

2.1. Conventional Reconstruction

Investigation of the interface between the Au nanorod and the SiO_2 shell and determination of the size and the orientation of the pores requires 3D characterization by electron tomography. Therefore, tilt series of HAADF-STEM images were acquired. **Figure 1**A presents a representative 2D HAADF-STEM image from the tilt series. When using HAADF-STEM, the signal is proportional to Z^n ($1.6 < n < 2$), n depending on the collection angle of the (HA)ADF-STEM detector.[19] In practice, the collection angle can be tuned within a specific range by changing the camera length of a given detector. Even more flexibility is provided in modern transmission electron microscopy (TEM) instruments, in which more than one (HA)ADF detector is often available. It is therefore possible to optimize the contrast between different elements through a careful selection of the collection angles.

In Figure 1A, the signal from the Au core is clear, but the intensity obtained from the shell is very weak due to the relatively low atomic number elements contained in SiO_2. The inner and outer collection angles of the HAADF detector used during the acquisition of the tilt series for electron tomography were 150 and 220 mrad, respectively. The collection angle was optimized to avoid diffraction effects, but clearly no information on the SiO_2 shell can be obtained when using these images as an input for 3D reconstruction. In order to obtain information from Au and SiO_2 simultaneously, smaller collection angles should be used. In Figure 1B, an annular dark-field (ADF)-STEM image is depicted, which was acquired using an ADF detector resulting in inner and outer collection angles of 35 and 125 mrad, respectively. It is clear that using this setup, both the Au core and the SiO_2 shell can be visualized. The Au nanorod appears to be homogeneously coated with the silica shell and one can observe that the shell has a porous morphology. A full tilt series of ADF-STEM images was acquired under the same conditions and used as an input for 3D reconstruction. A 3D visualization of the reconstruction, as well as an orthoslice through the reconstruction, is presented in **Figure 2** and an animated video is available in the Supporting Information. Orthoslices through the 3D reconstruction along the XZ and XY orientations (Figure 2A,B) clearly show the presence of artifacts, which can be seen as dark areas and streaks in the vicinity of the Au nanorod. Also in the 3D visualizations (Figure 2C,D), the artifacts are obvious. These artifacts appear due to a combination of the reasons listed below.

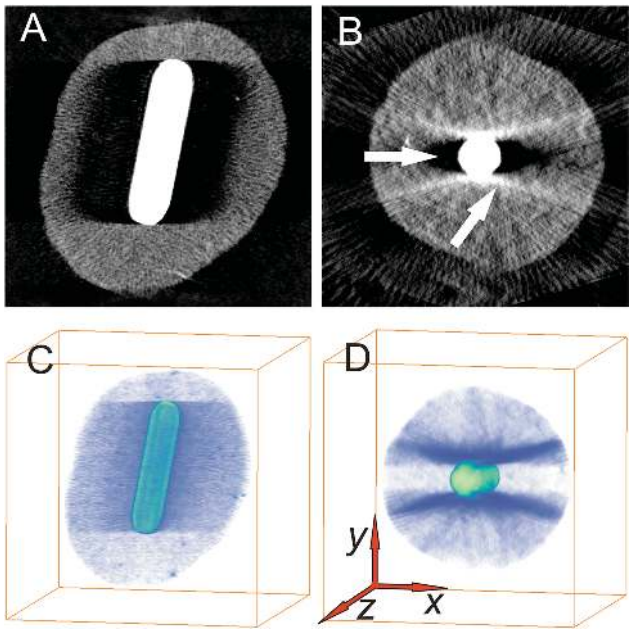

Figure 2. Reconstruction of a PTW Au@SiO_2 particle, using an ADF-STEM tilt series. A,B) Slices through the silica-coated PTW Au nanorod viewed in *XZ* (A) and *XY* (B) orientations. Dark and streaking artifacts can be observed in the vicinity of the Au nanorod and are highlighted with white arrows. C,D) Volume renderings of the ADF-STEM reconstruction viewed along *XZ* and *XY* orientations. The Au nanorod is depicted in light green and the surrounding silica is shown in blue. Although information from silica is present in the reconstruction, the resolution of the reconstruction is limited by the artifacts.

1) Diffraction contrast: artifacts originate because of the crystalline nature of the PTW Au nanorod. Such type of metal streak artifacts are also encountered in X-ray computed tomography (CT)[8,9] and caused by nonlinear attenuated projection data.
2) High contrast in 2D projection images: high contrast artifacts are often encountered when using fiducial Au markers in biological tomography series. These artifacts were already described in a previous study.[20] Here, a high contrast difference is present between the Au nanorod and SiO_2 in the HAADF-STEM images.

Since the observed artifacts may cause loss of information or may lead to misinterpretation, it is extremely challenging to obtain reliable 3D results for core–shell hybrid materials using conventional electron tomography. When selecting an optimal value for the collection angle, a compromise is needed between optimal contrast, produced by the atomic number of coexisting elements, and the minimization of diffraction contrast.

Part. Part. Syst. Charact. **2015**,
DOI: 10.1002/ppsc.201500097

2.2. Optimization of Acquisition of Tilt Series

A possible approach to solve the problem is the acquisition of two tilt series for this type of core–shell nanoparticles: one series with a low collection angle to obtain information from the part of the sample containing low atomic number elements and a second series at higher collection angle such that diffraction effects are removed. However, such an experiment would acquire double the amount of incoming electrons and as a consequence, the morphology of the hybrid structure might be different during the acquisition of the first and second tilt series because of electron beam damage. This will be especially problematic in the case of sensitive materials, such as the mesoporous shell surrounding the Au nanorod. We here overcome this limitation by exploiting the flexibility of modern TEM instruments that enable one to collect multiple (HA) ADF-STEM series simultaneously, by using different (HA) ADF detectors at the same time. In this manner, one is able to simultaneously collect two tilt series while keeping the necessary electron dose the same. As such, this multimode approach is very dose efficient. Tilt series were simultaneously acquired using an ADF detector with inner and outer collection angles of 35 and 125 mrad and a HAADF-STEM detector using inner and outer collection angles of 150 and 220 mrad, respectively.

2.3. Optimization of the 3D Reconstruction Procedure

To remove the artifacts that appear in the ADF-STEM tilt series, we propose an approach in which the complete Au nanoparticle is removed from the ADF-STEM projection images. First, the pixels corresponding to the Au nanorod were selected in the projection images of HAADF-STEM by applying a threshold. According to their histograms, the projection images were segmented into three regions; the core, the shell, and the surrounding C grid. As expected, the intensity values of the core were found to be higher in comparison to the shell. The threshold for masking was set to a value slightly higher than the intensity of the areas consisting of SiO_2. For other types of hybrid materials, this threshold value can be similarly determined, based on the compound with lowest intensity. Subsequently, the selected pixels for the Au core were removed from the projection images (**Figure 3**B) and replaced by a new intensity value as described below.

In order to achieve maximum correspondence between the selected (removed) region for the Au nanorod and its surrounding in each of the projection images, a technique known as "inpainting" was applied. This approach replaces the absent information by a continuation of the texture of the surrounding area. Inpainting has already been applied successfully in the field of X-ray tomography[21,22] and during cryo-electron tomography experiments in order to reduce metal originated artifacts.[20] In this paper, we focus on the inpainting method implemented in the Matlab software package. More technical details can be found in ref. [23] and [24]. This function fills the missing data (represented by a pixel mask) by iteratively propagating the available information at the boundaries into the area in which data are missing. In order to obtain a good correspondence between the recreated (inpainted) region and the SiO_2 shell,

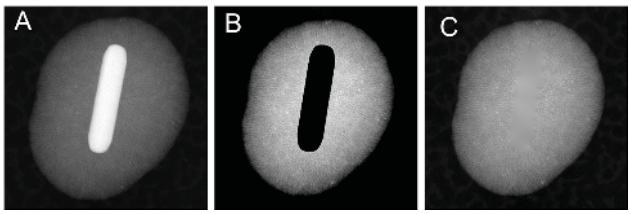

Figure 3. Different steps toward the optimization of the reconstruction of a ADF-STEM tilt series. A) Image acquired using ADF-STEM. B) After image segmentation, the pixels corresponding to the Au nanorod in SiO_2 were removed. C) Final image after the inpainting procedure. The removed pixels were replaced by the surrounding texture.

200 inpainting iterations were applied. This procedure was performed for each projection image of the tilt series separately, one representative image being depicted in Figure 3C. The full tilt series that was obtained in this manner is presented in the Supporting Information.

The processed tilt series was then used as an input for 3D reconstruction using the SIRT algorithm implemented in the All Scale Tomographic Reconstruction Antwerp (ASTRA) toolbox. Slices through the 3D reconstruction based on the modified ADF-STEM series are presented in **Figure 4**A,B, along the *XZ* and *XY* orientations, respectively. From these reconstructions, the porous structure of the shell is clearly observed and artifacts are greatly reduced as compared to Figure 2.

Finally, the 3D HAADF-STEM and ADF-STEM reconstructions are combined into one single visualization using the

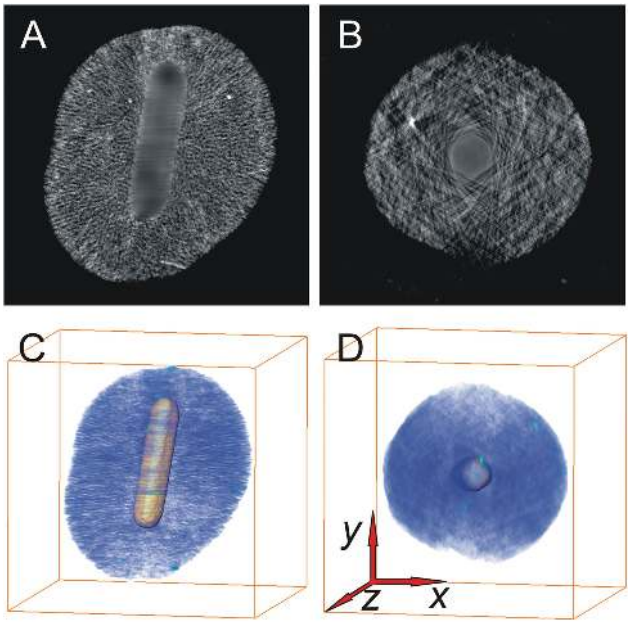

Figure 4. 3D reconstruction of PTW Au@SiO_2 using ADF-STEM and HAADF-STEM tomography. The Au nanorod and silica shell are displayed in yellow and blue, respectively. The reconstruction was obtained using HAADF-STEM tomography for the Au core and by ADF-STEM for the silica shell. A) Orthoslices through the mesoporous silica shell, viewed in XZ and XY orientation. After optimization of reconstruction, dark and streaking artifacts (see Figure 2A,B) were eliminated. C,D) Volume renderings of the ADF-STEM reconstruction viewed along XZ and XY orientations. The pores and channels can be clearly visualized.

AMIRA software.[25] The result of this procedure is presented in Figure 4C,D. In Figure 4C, the reconstruction of the Au nanorod was obtained via HAADF-STEM tomography. The surrounding SiO_2 was reconstructed using ADF-STEM tomography with an optimization of reconstruction algorithm. An animated video and the slices of the reconstructions are provided in the Supporting Information. After careful investigation, we conclude that the pores are mainly originating from the surface of the Au nanorod and the pore channels are oriented in a radial manner. Furthermore, the quality of the reconstruction enables us to estimate the average pore size, which was determined to be 2.5 nm (±0.4 nm).

Using the optimized approach for electron tomography that we present here, we were able to minimize the loss of information in the vicinity of the Au nanorod, yielding a full characterization of the 3D structure of the Au-SiO_2 hybrids. Such 3D investigation could not be obtained using conventional tomography. One can expect missing information in the final SiO_2 reconstruction because of the removal of the Au nanorod from the projection images. Indeed, due to the overlap of Au and SiO_2 in the 2D HAADF-STEM projection images, the removed pixels contain information from both Au and SiO_2. Nevertheless in the final reconstruction, the effect of such missing information was not prevalent. A likely explanation is that the removed intensity values were strongly dominated by the contribution of the intensity originating from the Au nanorod and a minor contribution from SiO_2 expected to be present. In addition, when the nanoparticle was tilted to higher/lower tilt angles, the previously removed information could be retrieved in the subsequent projections. We could consider that the effect of the procedure we propose here is equivalent to the effect of a small missing wedge. Given the dominant nature of the artifacts as presented in Figure 2, the effect of removing pixels that contain intensity from the SiO_2 is much less significant.

3. Conclusions

In this study we proposed a novel approach to reconstruct the structure of hybrid core–shell nanomaterials. Both the acquisition and reconstruction during an electron tomography experiment were hereby optimized. Tilt series were acquired in a dose-efficient manner by simultaneously collecting images using two different (HA)ADF-STEM detectors. Furthermore, an advanced masking and inpainting procedure was applied to remove artifacts that are present in a conventional tomography reconstruction. In this manner, we were able to reliably characterize the structure of mesoporous silica coated PTW Au nanorods. It must be noted that the methodology we propose here is generally applicable to a broad range of core–shell hybrid nanostructures.

4. Experimental Section

Materials: The synthesis of PTW Au nanorods was carried out following a previously reported protocol.[26] Coating with mesoporous SiO_2 was obtained by a surfactant-templated synthesis adapted from the Stöber method were the PTW nanorods acted as the nucleation site. Cetyltrimethylammonium bromide was used as surfactant and tetraethoxysilane as the silica source.[27]

Characterization and Instrumentation: Samples for TEM were prepared by casting drops of ethanol suspension containing the PTW Au@mSiO_2 nanoparticles on a quantifoil carbon TEM grid. The grid was placed in a model 2020 Fischione Instruments tomography holder. Tilt series were recorded using a FEI Tecnai Osiris electron microscope at an operating voltage of 120 kV. The probe convergence semiangle equalled 7 and a camera length of 34 mm was selected to obtain incoherent image formation using a HAADF-STEM detector corresponding to inner and outer collection semiangles of 150 and 220 mrad, respectively. ADF-STEM images were acquired using a different detector present in the column. A camera length of 34 mm was used yielding inner and outer semiangles of 35 and 125 mrad, respectively. Tilt series of HAADF-STEM and ADF-STEM images were simultaneously recorded at angles ranging from +74° to −73° with a 3° increment. The projection images were aligned using a cross-correlation algorithm together with a manual tilt axis adjustment implemented in the FEI Inspec3D software.[28] Both tilt series were aligned using the same shifts and tilt axis adjustments. After additional processing, as explained in Section 2.3, the tilt series were reconstructed via SIRT implementation of the ASTRA tomography toolbox[29,30] with 100 iterations. For 3D visualizations, the Amira software was used. For the Au nanoparticle an isosurface rendering was used and, in order to visualize the silica, a volume rendering was applied. Hereby, a low alpha-scale was used in order to obtain sufficient transparency such that the Au nanoparticle remains visible.

Supporting Information

Supporting Information is available from the Wiley Online Library or from the author.

Acknowledgements

S.B. acknowledges financial support from European Research Council (ERC) (ERC Starting Grant No. 335078-COLOURATOM). L.-M. acknowledges funding from the EU, Grant No. 310651-2 Self-Assembly in Confined Space (SACS). K.J.B. acknowledges financial support from the Netherlands Organisation for Scientific Research (NWO), Project No. 639.072.005 and NWO CW 700.57.026. Networking support was provided by COST Action MP1207. The authors acknowledge the European Union under the Seventh Framework Program under a contract for an Integrated Infrastructure Initiative, Reference No. 312483-ESTEEM2 for financial support.

Received: June 26, 2015
Revised: August 31, 2015
Published online:

[1] P. Midgley, M. Weyland, *Ultramicroscopy* **2003**, *96*, 413.
[2] P. A. Midgley, R. E. Dunin-Borkowski, *Nat. Mater.* **2009**, *8*, 271.
[3] A. J. Koster, U. Ziese, A. J. Verklij, A. H. Janssen, K. P de Jong, *J. Phys. Chem.* **2000**, *104*, 9368.
[4] S. Bals, G. Van Tendeloo, C. Kisielowski, *Adv. Mater.* **2006**, *18*, 892.
[5] B. Goris, S. Bals, W. Van den Broek, J. Verbeeck, G. Van Tendeloo, *Ultramicroscopy* **2011**, *111*, 1262.
[6] K. Lu, E. Sourty, J. Loos, *J. Electron Microsc.* **2010**, *59*, 39.
[7] H. Friedrich, M. R. McCartney, P. R. Buseck, *Ultramicroscopy* **2005**, *106*, 18.
[8] M. Cao, H.-B. Zhang, Y. Lu, R. Nishi, A. Takaoka, *J. Microsc.* **2010**, *239*, 66.

[9] F. E. Boas, D. Fleischmann, *Imaging Med.* **2012**, *4*, 229.
[10] S. J. Pennycook, *Annu. Rev. Mater. Sci.* **1992**, *22*, 171.
[11] P. Gilbert, *J. Theor. Biol.* **1972**, *36*, 105.
[12] B. Goris, W. Van den Broek, K. J. Batenburg, H. H. Mezerji, Sara Bals, *Ultramicroscopy* **2012**, *113*, 120.
[13] R. Leary, Z. Saghi, P. A. Midgley, D. J. Holland, *Ultramicroscopy* **2013**, *131*, 70.
[14] K. J. Batenburg, S. Bals, C. Kubel, P. Midgley, J. C. Hernandez, U. Kaiser, E. R. Encina, E. A. Coronado, G. Van Tendeloo, *Ultramicroscopy* **2009**, *109*, 730.
[15] E. Carbó-Argibay, B. Rodriguez-Gonzalez, I. Pastoriza-Santos, L. M. Liz-Marzan, *Nanoscale* **2010**, *2*, 2377.
[16] L. M. Liz-Marzan, M. Giersig, P. Mulvaney, *Langmuir* **1996**, *12*, 4329.
[17] P. C. Angelomé, I. Pastoriza-Santos, J. Perez-Juste, B. Rodriguez-Gonzalez, A. Zelcer, J. Galo, A. A. Soler-Illia, L. M. Liz-Marzan, *Nanoscale* **2012**, *4*, 931.
[18] P. C. Angelomé, I. Pastoriza-Santos, J. Perez-Juste, B. Rodriguez-Gonzalez, A. Zelcer, J. Galo, A. A. Soler-Illia, L. M. Liz-Marzan, *J. Sol–Gel Sci. Technol.* **2014**, *70*, 180.
[19] P. Hartel, H. Rose, C. Dinges, *Ultramicroscopy* **1996**, *63*, 93.
[20] K. Song, L. R. Comolli, M. Horowitz, *J. Struct. Biol.* **2012**, *178*, 108.
[21] Y. Chen, L. Yinsheng, H. Guo, Y. Hu, L. Luo, X. Yin, J. Gu, C. Toumoulin, *Math. Probl. Eng.* **2012**, *2012*, 786281
[22] J. Gu, L. Zhang, G. Yu, Y. Xing, Z. Chen, *J. X-Ray Sci. Technol.* **2006**, *14*, 73.
[23] D. Garcia, *Comput. Stat. Data Anal.* **2010**, *54*, 1167.
[24] G. Wang, D. Garcia, Y. Liu, R. de Jeu, A. J. Dolman, *Environ. Modell. Softw.* **2012**, *30*, 139.
[25] D. Stalling, M. Westerhoff, H.-C. Hege, in *The Visualization Handbook*, (Eds: C. D. Hansen and C. R. Johnson), Academic Press, Elsevier, **2004**, pp. 749–767.
[26] J. Pérez-Juste, L. M. Liz-Marzan, S. Carnie, D. Y. C. Chan, P. Mulvaney, *Adv. Funct. Mater.* **2004**, *14*, 571.
[27] M. N. Sanz-Ortiz, K. Sentosun, S. Bals, L. M. Liz-Marzán, *ACS Nano* **2015**, DOI:10.1021/acsnano.5b04744.
[28] R. H. M. Schoenmakers, R. A. Perquin, T. F. Fliervoet, W. Voorhout, *Microsc. Microanal.* **2005**, *11*, 312.
[29] W. J. Palenstijn, K. J. Batenburg, J. Sijbers, *J. Struct. Biol.* **2011**, *176*, 250.
[30] W. Van Aarle, W. J. Palenstijn, J. De Beenhouwer, T. Altantzis, S. Bals, K. J. Batenburg, J. Sijbers, *Ultramicroscopy* **2015**, *157*, 35.